# A low climate threshold for south Greenland Ice Sheet demise during the Late Pleistocene

Nil Irvali[a,b,1], Eirik V. Galaasen[a,b], Ulysses S. Ninnemann[a,b], Yair Rosenthal[c,d], Andreas Born[a,b], and Helga (Kikki) F. Kleiven[a,b]

[a]Department of Earth Science, University of Bergen, 5007 Bergen, Norway; [b]Bjerknes Centre for Climate Research, 5007 Bergen, Norway; [c]Department of Marine and Coastal Sciences, Rutgers, State University of New Jersey, New Brunswick, NJ 08901; and [d]Department of Earth and Planetary Sciences, Rutgers, State University of New Jersey, New Brunswick, NJ 08901

Edited by Gilles Ramstein, Laboratoire des Sciences du Climat et de l'Environnement, Gif-Sur-Yvette, France, and accepted by Editorial Board Member Jean Jouzel November 4, 2019 (received for review July 11, 2019)

**The Greenland Ice Sheet (GIS) has been losing mass at an accelerating rate over the recent decades. Models suggest a possible temperature threshold between 0.8 and 3.2 °C, beyond which GIS decline becomes irreversible. The duration of warmth above a given threshold is also a critical determinant for GIS survival, underlining the role of ocean warming, as its inertia prolongs warmth and triggers longer-term feedbacks. The exact point at which these feedbacks are triggered remains equivocal. Late Pleistocene interglacials provide potential case examples for constraining the past response of the GIS to a range of climate states, including conditions warmer than present. However, little is known about the magnitude and duration of warming near Greenland during these periods. Using high-resolution multiproxy surface ocean climate records off southern Greenland, we show that the previous 4 interglacials over the last ∼450 ka all reached warmer than present climate conditions and exceeded the modeled temperature threshold for GIS collapse but by different magnitudes and durations. Complete deglaciation of the southern GIS in Marine Isotope Stage 11c (MIS 11c; 394.7 to 424.2 ka) occurred under climates only slightly warmer than present (∼0.5 ± 1.6 °C), placing the temperature threshold for major GIS retreat in the lower end of model estimates and within projections for this century.**

Greenland Ice Sheet | Late Pleistocene interglacials | climate change | thresholds

Understanding the response of the Greenland Ice Sheet (GIS) to global warming is consequential, as the complete melting of the GIS can contribute up to 7 m of global sea-level rise (1). While the relative amounts of GIS retreat during recent interglacials remains somewhat equivocal, emerging results suggest that the size and discharge of GIS varied significantly both within and between recent interglacial periods. In Marine Isotope Stage 5e (MIS 5e) and MIS 11c, GIS retreat likely contributed 0.4 to 5.6 and 3.9 to 7.0 m, respectively, to sea-level rise above present (2–4). The latter implies that a substantial portion of the GIS was lost in MIS 11c, consistent with the presence of spruce forests and the cessation of Greenland silt discharge interpreted to reflect complete deglaciation of the southern GIS (5, 6). Bedrock data suggest that even central Greenland was ice free in one or more recent interglacials (7). Ice likely remained over southern Greenland in MIS 5e, MIS 7e, and MIS 9e, despite intervals of increased sediment discharge from Precambrian Greenland (PG) terranes, indicating elevated GIS activity and retreat, particularly in MIS 9e (8, 9). In the Holocene, by contrast, the GIS appears to have been relatively large and unusually stable (9). Thus, the response of the GIS to Late Pleistocene interglacial climate forcings varied substantially and included increased melting during 3 of the 4 recent interglacials compared with the Holocene (9) and near full retreat during MIS 11c.

Resolving the climate conditions associated with these different GIS responses is crucial for understanding the processes and thresholds determining past GIS retreat and survival. Yet, the climatic background associated with and driving these changes remains poorly constrained. Dinocyst-based sea surface temperature (SST) records suggest variable interglacial warmth during Late Pleistocene interglacials close to southern Greenland (5). However, there are no available SST records proximal to southern Greenland that span all recent interglacials, including MIS 9e, which is a particularly interesting interval given strong but incomplete GIS retreat (9).

Here, we provide high-resolution ocean climate (SST) reconstructions from Integrated Ocean Drilling Program (IODP) Site U1305 (57°28.5′ N, 48°31.8′ W; 3,459 m) from the Eirik Drift off southern Greenland, spanning MIS 7e (benthic $\delta^{18}O$ plateau: 232.6 to 243.2 ka), MIS 9e (benthic $\delta^{18}O$ plateau: 320.9 to 333.1 ka), and MIS 11c (benthic $\delta^{18}O$ plateau: 394.7 to 424.2 ka), which we combine with existing MIS 5e (benthic $\delta^{18}O$ plateau: 117.9 to 128.2 ka) records from this location (Core MD03-2664) (10). This site is sensitively situated to monitor subpolar climate near and partially over Greenland (*SI Appendix*, Fig. S1), fluctuations in GIS extent, and iceberg calving events (10, 11). We use benthic foraminifera $\delta^{18}O$ to identify peak interglacial intervals and constrain our age model (*SI Appendix*, Fig. S2). Changes in climate are portrayed using planktonic foraminiferal $\delta^{18}O$, assemblage counts, modern analog technique (MAT)-derived SSTs, and Mg/Ca paleothermometry using *Neogloboquadrina pachyderma*

## Significance

**Understanding how warmer climates affected Greenland in the past helps in determining how future warming will impact it. The Greenland Ice Sheet (GIS) has retreated during recent interglacials, suggesting a critical survival threshold within a few degrees of modern temperatures. Defining this temperature threshold requires records of the past climates responsible for GIS demise. Using microfossil temperature reconstructions, we show that the current interglacial is unusually moderate and that all 4 previous interglacials were warmer than present near Greenland. Both magnitude and duration of past warmth were important influences on the ice sheet. Notably, the critical temperature threshold for past GIS decay will likely be surpassed this century. The duration for which this threshold is exceeded will determine Greenland's fate.**

Author contributions: U.S.N. designed research; N.I., E.V.G., Y.R., and A.B. performed research; N.I., E.V.G., U.S.N., Y.R., and A.B. analyzed data; and N.I., E.V.G., U.S.N., Y.R., A.B., and H.(K.)F.K. wrote the paper.

The authors declare no competing interest.

This article is a PNAS Direct Submission. G.R. is a guest editor invited by the Editorial Board.

This open access article is distributed under Creative Commons Attribution-NonCommercial-NoDerivatives License 4.0 (CC BY-NC-ND).

[1]To whom correspondence may be addressed. Email: nil.irvali@uib.no.

This article contains supporting information online at https://www.pnas.org/lookup/suppl/doi:10.1073/pnas.1911902116/-/DCSupplemental.

First published December 23, 2019.



Downloaded at UNIVERSITETSBIBL I BERGEN TIDSSKRIFT on January 14, 2020

(sinistral) and *Neogloboquadrina incompta* (Fig. 1). Ice-rafted debris (IRD) counts and planktonic foraminifer Ba/Ca are further used to infer iceberg supply and melt water input (12) (Fig. 2).

## Results and Discussion

Our SST records (Figs. 1 and 3) show that all 4 previous interglacials were at least as warm as present south of Greenland, albeit with varying degrees of excess warmth. The mean MAT summer SSTs through the interglacial plateaus indicate that MIS 9e was the warmest (~11 °C) of the previous 4 interglacials followed by MIS 5e (~9.3 °C), MIS 11c (~8.1 °C), and MIS 7e (~7 °C). For reference, modern MAT summer SSTs at the site are 7.7 °C (*SI Appendix*). Peak temperatures during each of the 4 most recent interglacials intermittently exceeded the modern (core top MAT SST) (Fig. 3). The duration of warmer than present conditions also varied widely between the interglacial $\delta^{18}O$ plateaus, with temperatures above present levels for 20.7 ka in MIS 11c, 12.2 ka in MIS 9e, 9.7 ka in MIS 5e, and 4.4 ka in MIS 7e. The distinct changes in relative abundance of foraminifer fauna further highlight the environmental (habitat) differences experienced between interglacials. In particular, MIS 9e stands out in terms of warm planktonic foraminifer fauna (*SI Appendix*, Fig. S3). The relative abundance of subpolar *N. incompta* reached a maximum of ~88% during late MIS 9e, and *N. pachyderma* (s) coiling ratio dropped to 0% for the only time in the last ~450 ka. Reduced *N. pachyderma* (s) coiling ratio is also observed during the peak warm periods of MIS 5e (~11%), MIS 7e (~48%), and MIS 11c (~42%). For context, the modern planktonic foraminiferal assemblage at Eirik Drift is dominated by the polar *N. pachyderma* (s) with core top coiling ratios reaching as high as 100% (*SI Appendix*, Fig. S4), similar to the last 2 ka (94%) and Holocene average (93%) (*SI Appendix*), revealing anomalously cold and stable conditions in the current interglacial that are not particularly representative of interglacials in general.

Comparing our climate records with previous reconstructions of GIS sediment discharge and retreat (6, 8, 9) reveals a clear pattern of high southern GIS melt (PG percentage and silt provenance records) when SSTs were high and polar fauna [*N. pachyderma* (s) coiling ratio] were low (Fig. 2), indicating that GIS activity was closely coupled to nearby ocean temperatures on centennial–millennial timescales. Thus, strong GIS melt and retreat occurred when subpolar temperatures exceeded current levels. However, the different magnitude and duration of interglacial warmth off of southern Greenland provide additional information for delineating the sensitivity of the GIS to climates warmer than today. The recent increase in GIS melting coincided with the onset of industrial era Arctic warming, but the magnitude of GIS melting has only recently emerged beyond the range of natural variability (13) and quadrupled over the past decade (14). Due to the nonlinear response of surface melting to increasing summer air temperatures, continued atmospheric warming will

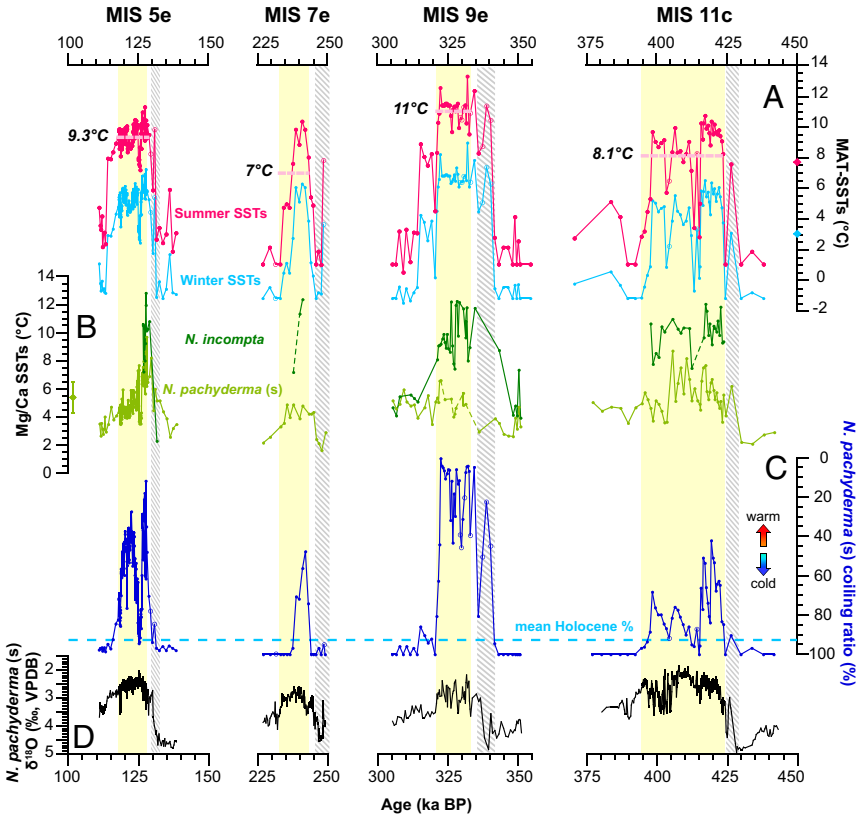


**Fig. 1.** SST records from Sites MD03-2664 (MIS 5e) and U1305 (MIS 7e, MIS 9e, and MIS 11c) spanning the last 450 ka. (*A*) MAT summer (pink) and winter (blue) SSTs. (*B*) Mg/Ca SSTs from *N. pachyderma* (s) (light green) and *N. incompta* (dark green). (*C*) *N. pachyderma* (s) coiling ratio (percentage). (*D*) *N. pachyderma* (s) $\delta^{18}O$ record. Core top MAT summer (pink diamonds), MAT winter (blue diamonds), and *N. pachyderma* (s) Mg/Ca (green diamonds) SSTs from the Eirik Drift Multicore GS06-144-03 MC A (18) are shown for comparison with modern SSTs at core site. In *A*, dashed light pink lines and SST values mark the mean MAT summer SSTs through the interglacial plateaus. The dashed light blue line in *C* marks the mean Holocene (last 9.5 ka) *N. pachyderma* (s) coiling ratio from the Eirik Drift Core MD03-2665 (*SI Appendix*). Open circles mark samples with low (<150) total number of planktonic foraminifera. Yellow shading marks the interglacial benthic $\delta^{18}O$ plateaus. Data points only within the interglacial benthic $\delta^{18}O$ plateaus (yellow shaded intervals) are included in the mean SST calculations (*Materials and Methods*). Gray (cross-hatched) shading marks deglacial IRD peaks (Heinrich events) (*SI Appendix*). VPDB, Vienna Pee Dee Belemnite.



Downloaded at UNIVERSITETSBIBL I BERGEN TIDSSKRIFT on January 14, 2020

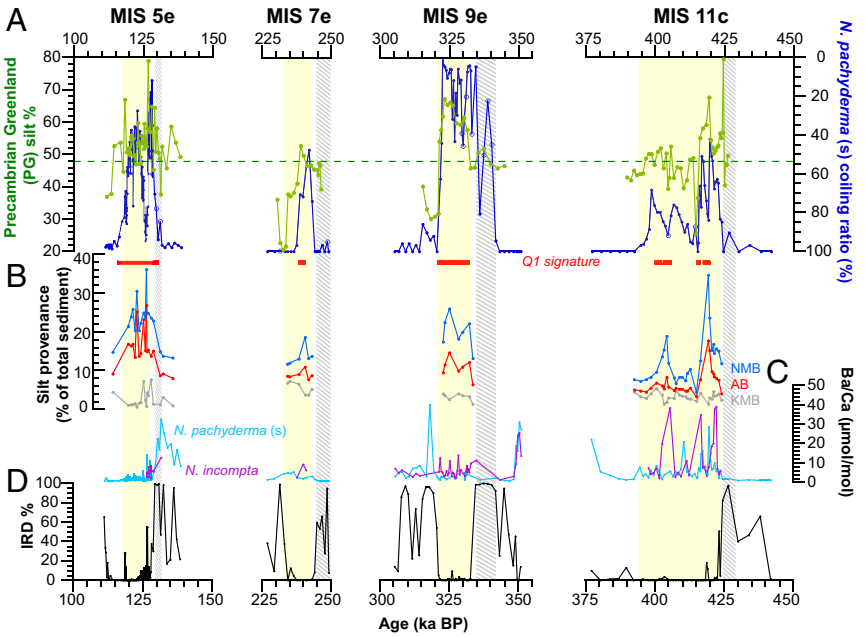


**Fig. 2.** Comparison with GIS discharge records. (*A*) Modeled PG percentage silt contributions (green) from Core MD99-2227 plotted together with *N. pachyderma* (s) coiling ratio (percentage; dark blue) from Sites MD03-2664 (10, 43) and U1305 spanning the last 450 ka. Open circles [in *N. pachyderma* (s) coiling ratio] mark samples with low (<150) total number of planktonic foraminifera. Duration of quadrant 1 (Q1) signatures (red bars) is used by Hatfield et al. (9) to mark intervals with strongest PG sourcing when silt wt % > 45% and PG% > 48%. The dashed green line in PG percentage marks 48%. (*B*) Silt provenance records expressed as percentage of total sediment derived from south Greenland's 3 Precambrian bedrock terranes (i.e., from south to north: Ketilidian Mobile Belt [KMB; gray], Archean Block [AB; red], and Nagssugtoqidian Mobile Belt [NMB; blue]) from Eirik Drift Core MD99-2227 (6, 8, 9). (*C*) *N. pachyderma* (s)-derived (light blue) and *N. incompta*-derived (purple) Ba/Ca. (*D*) IRD percentage from Sites MD03-2664 (10, 43) and U1305 spanning the last 450 ka. Yellow shading marks the interglacial benthic $\delta^{18}$O plateaus. Gray (cross-hatched) shading marks deglacial IRD peaks (Heinrich events).

further accelerate the melting (13). Models suggest that GIS demise is inevitable after a certain temperature threshold is passed (15, 16). Robinson et al. (16) estimate a warming threshold for an ice-free Greenland to be in the range of 0.8 to 3.2 °C, with a best estimate of 1.6 °C warming relative to preindustrial climate. However, crossing the temperature threshold does not necessarily lead to a rapid GIS collapse, and the time needed to melt a significant portion of the GIS may be strongly dependent on the level

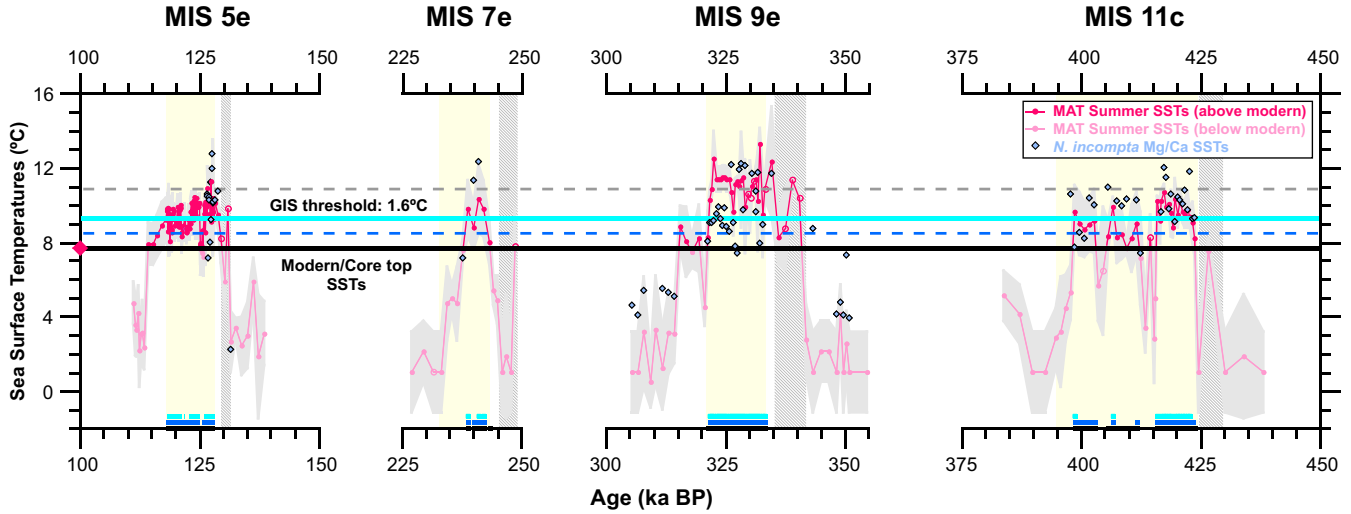


**Fig. 3.** GIS thresholds. MAT summer and *N. incompta* Mg/Ca SSTs (light purple diamonds) spanning the last 450 ka. The pink diamond and the black bold line mark the modern/core top MAT summer SST (7.7 °C) from the Eirik Drift Multicore GS06-144-03 MC A (*SI Appendix*). MAT summer SSTs above modern temperature are shown in dark pink, and MAT summer SSTs below modern temperature are shown in light pink. Light gray shading marks the uncertainty (i.e., the SD of the estimates from the top 5 analogs) in MAT summer SSTs. Open circles mark samples with low (<150) total number of planktonic foraminifera. Yellow shading marks the interglacial benthic $\delta^{18}$O plateaus. Gray (cross-hatched) shading marks deglacial IRD peaks (e.g., Heinrich events). The bold light blue line and the dashed blue and gray lines mark the modeled global mean temperature threshold for the GIS collapse (1.6 °C) and its range (0.8 to 3.2 °C), respectively (16). Black, dark blue, and light blue bars (along the bottom) mark the durations of MAT summer SSTs above modern, 0.8 °C threshold, and 1.6 °C threshold, respectively.



Downloaded at UNIVERSITETSBIBL I BERGEN TIDSSKRIFT on January 14, 2020

of warming (3, 15, 17). In order to further explore GIS thresholds, we apply the 1.6 °C (0.8 to 3.2 °C) warming threshold of Robinson et al. (16) to our SST records (Fig. 3). According to our MAT summer SSTs, all of the previous 4 interglacials over the last ∼450 ka intermittently exceeded the modeled temperature threshold of 1.6 °C suggested for GIS collapse. Within the interglacial $\delta^{18}O$ plateaus, SSTs stayed above the 1.6 °C threshold for 11.7 ka in MIS 9e, 8.7 ka in MIS 11c, 5.8 ka in MIS 5e, and 3.0 ka in MIS 7e. MAT summer SSTs at the Eirik Drift never reached the 1.6 °C warming threshold during the last 2 ka or any other time during the Holocene (*SI Appendix*) (18).

Comparison of MIS 5e, MIS 9e, and MIS 11c is particularly interesting, since ice persisted on southern Greenland during both MIS 5e and MIS 9e, whereas it was nearly completely deglaciated during MIS 11c (6, 8, 9). Yet, our MAT summer SST records suggest that MIS 9e was the warmest of the previous 4 interglacials and that SSTs stayed above the 1.6 °C threshold the longest throughout the interglacial plateau (Fig. 3). Elevated southern GIS sediment discharge during the MIS 9e warmth (Fig. 2) may suggest that the ice sheet responded, but retreat was limited compared with MIS 11c (9). The contrast between the near-complete deglaciation of southern GIS during the moderate warming of MIS 11c and a persistent southern GIS during the warmer MIS 9e has implications for the critical factors determining GIS size. An ice-free southern GIS during MIS 11c suggests that southern GIS survival was strongly dependent on the duration of warmer than present conditions rather than crossing the modeled (1.6 °C) temperature threshold for the GIS collapse. For example, taking a lower temperature threshold of 0.8 °C, the lower limit of the estimate of Robinson et al. (16), could help explain strong retreat during MIS 11c. MIS 11c was over the 0.8 °C limit longer (∼14.9 ka) than any other Late Pleistocene interglacial, including for ∼3 ka longer than the warmer MIS 9e (Table 1).

Of course, there may not be a single uniformly applicable temperature threshold for GIS survival. GIS mass balance also depends on other factors, such as geometry, accumulation, and moisture supply, which in turn, are related to SSTs and sea ice extent (19). Thus, a number of mechanisms could explain why the degree, or even the sign, of the mass balance response to warming is time sensitive. For example, warming may initially increase accumulation locally (and in particular, in southeast Greenland) (20) but also, decrease ice viscosity (via liquid water and warming), resulting in slow dynamic feedbacks eventually driving mass loss (21). In addition to dynamics, the apparent long response time for removal of the southern and eastern central GIS might simply reflect the inherent stability of this region due to its high mass turnover (accumulation–ablation). In this region, surplus melting due to a warmer climate does not represent a large relative imbalance to natural fluxes (22, 23). Using the temperature dependence of the surface mass balance from idealized simulations with a comprehensive model (20), we estimate the resilience of different regions of the GIS (*SI Appendix*, Fig. S5). The accelerating surface warming due to the ice-elevation feedback reaches a tipping point where a reversal of the initial warming is not enough to stop further ice loss. Large regions in northern and western Greenland destabilize quickly, whereas large parts of the ice margin along the eastern coast are less vulnerable, requiring up to 10 ka to reach a tipping point.

## Conclusions

The current interglacial seems to have been notably stable and mild off southern Greenland, perhaps explaining the relative stability and large size of the GIS during the Holocene, while also skewing our concept of the "natural" interglacial size and stability of this ice sheet (9, 24). By corollary, each of the previous 4 interglacials was warmer than the Holocene by varying degrees. We suggest that these conditions can explain both the interglacial size and the evolution of the southern GIS, where the duration of warming relative to the modern climate seems to have been as important as the magnitude, at least beyond a critical threshold value. Our reconstructions suggest that temperatures in the lower range of the modeled warming threshold (∼0.8 °C) (3), within the range of projections for this century, were enough to cause southern GIS disintegration during MIS 11c. A low GIS threshold increases the plausibility that one of the most economically impactful (25) long-term consequences of warming could be passed well below the 2 °C threshold and may already be unavoidable if even modestly warmer conditions were to persist long enough (26).

## Materials and Methods

**Sample Preparation.** Site U1305 was recovered during IODP Expedition 303 off southern Greenland. The core was sampled continuously with 2-cm sample spacing over the interglacial periods MIS 7e (43.85 to 49.75 meters composite depth [mcd]), MIS 9e (54.99 to 63 mcd), and MIS 11c (63.8 to 80.03 mcd). Samples were soaked in distilled water and left overnight on a shaker to disperse the sediment. All samples were wet sieved using a 63-μm-sized sieve.

**Table 1. GIS thresholds summary**

| | MIS 5e | MIS 7e | MIS 9e | MIS 11c |
|---|---|---|---|---|
| Age range (ka) of MIS plateaus* (based on LR04) | 117.9–128.2 | 232.6–243.2 | 320.9–333.1 | 394.7–424.2 |
| Rough amplitude of southern GIS retreat† | Medium (8) | Small (9) | Medium (9) | Large (5, 6, 9) |
| Mean summer SSTs through MIS plateaus, °C | 9.3 | 7.0 | 11.0 | 8.1 |
| Mean measure of GIS discharge‡ | High | Low | High | Low |
| Duration (ka) of warming above modern SSTs | 10.2 [11.5]§ | 5.5 | 12.0 [15.6]§ | 20.2 |
| Duration (ka) of warming above 0.8 °C threshold | 9.4 [10.4]§ | 4.8 | 11.9 [14.7]§ | 14.9 |
| Duration (ka) of warming above 1.6 °C threshold | 5.8 [6.5]§ | 3.0 | 11.7 [14.2]§ | 8.7 |

*MIS plateaus (i.e., the periods of low and relatively constant ice volume) are defined based on our epibenthic foraminifera *Cibicidoides wuellerstorfi* $\delta^{18}O$ records (*SI Appendix*, Fig. S2).

†Small indicates minimal southern GIS retreat (southern GIS did not retreat from the shelf) (9). Medium indicates extensive southern GIS retreat, but ice remained on each south Greenland PG terrane (8, 9). Large indicates near-complete deglaciation of southern GIS (5, 6, 9).

‡Based on PG silt percentage and duration of quadrant 1 (Q1) signatures (high PG percentage and high silt content) in Eirik Drift Core MD99-2227 after Hatfield et al. (9).

§The duration of warming was estimated based on MAT-derived summer SSTs using only data within the MIS plateaus (e.g., yellow shaded intervals in Fig. 3). However, SSTs were intermittently high prior to the beginning of the MIS 5e plateau (at ∼129.5 ka) and the MIS 9e plateau (at ∼336.7 ka). If these intermittent warmings are included (and the duration is extended to 117.9 to 129.5 ka for MIS 5e and 320.9 to 336.7 ka for MIS 9e; to include part of the deglacial), the MIS 5e and MIS 9e interval of warmth is longer (shown in brackets). Note, however, that this does not influence the ranking of interglacials according to the duration of warming.



Downloaded at UNIVERSITETSBIBL I BERGEN TIDSSKRIFT on January 14, 2020

The coarse fraction (>63 μm) was dry sieved and further used for stable isotope analysis, foraminiferal assemblages, IRD counts, and Mg/Ca analysis.

**Stable Isotopes.** Stable isotope analyses ($\delta^{18}O$ and $\delta^{13}C$) were performed on the planktonic foraminifer species *N. pachyderma* (sinistral) in order to reconstruct surface ocean physical and chemical properties. *N. pachyderma* (s) tests were picked every 4 cm (with notable gaps due to absence, particularly in MIS 9e) from the 150- to 212-μm-sized fraction (7 to 12 specimens per analysis) and measured twice per sample when the abundance allowed (~92% of the total 616 samples measured).

A Finnigan MAT253 mass spectrometer, located at the Facility for Advanced Isotopic Research and Monitoring of Weather, Climate and Biogeochemical Cycling, Department of Earth Science, University of Bergen, was used for the stable isotope analysis. Averages of the replicate measurements are shown in the results, and values are reported relative to Vienna Pee Dee Belemnite, calibrated using National Bureau of Standards (NBS)-19 and cross-checked with NBS-18. During the analysis period, the long-term reproducibility (1σ) values of in-house standards for samples between 10 and 100 μg were better than 0.08 and 0.04‰ for $\delta^{18}O$ and $\delta^{13}C$, respectively.

**Foraminiferal Assemblages and IRD Counts.** Foraminiferal assemblage and IRD counts for Site U1305 were performed at every 16-cm resolution through MIS 9e and every 32 cm through MIS 7e and MIS 11c. The >150-μm fraction was used for foraminiferal assemblages and IRD counts. After additional dry sieving, samples were split, and at least 300 planktonic foraminifera were counted. The total number of foraminifera was too low (<150) for 2 samples from MIS 5e, MIS 7e, and MIS 11c and 7 samples from MIS 9e. For completeness, these samples are shown but denoted with open circles in Figs. 1–3 and *SI Appendix*, Figs. S3, S6, and S7. However, they are not included when estimating mean summer MAT SSTs (Fig. 1 and Table 1) and duration of warming (Fig. 3 and Table 1), since percentage values can be overestimated when abundances are low (*SI Appendix* has more discussion of these low-foraminifera abundance–high-IRD intervals). Note that including (or excluding) these points does not, however, affect any of our main results or conclusions. The most abundant species were *N. pachyderma* (s), *N. incompta*, *Turborotalia quinqueloba*, *Globigerina bulloides*, and *Globigerinita glutinata*. We calculate the coiling ratio of *N. pachyderma* (s) as the percentage of the sinistral coiling variety in total *N. pachyderma* (sinistral + dextral coiling)). *N. pachyderma* (s) coiling ratio has been used as an SST proxy at high latitudes (10), as the sinistral coiling *N. pachyderma* is abundant in cold/polar regions, whereas the dextral coiled form prefers more temperate/subpolar regions. We follow the definition by Darling et al. (27) and refer to the dextral coiled *N. pachyderma* specimens as *N. incompta* (i.e., when the dextral coiling ratio is between 3 and 97%).

IRD grains in the >150-μm fraction were also counted. The percentage of IRD grains in total entities (i.e., foraminifera) was calculated and used as an indicator of iceberg discharge to the study area. At least ~300 grains were counted.

**MAT SSTs.** Here, we use the MAT to reconstruct SSTs from the assemblages of planktonic foraminifera (28, 29) (Fig. 1). We use the modern North Atlantic core top planktonic foraminiferal assemblage database (862 samples) compiled by the MARGO Project (30). Following Kucera et al. (30), we compute the modern SST values at sample locations using the World Ocean Atlas (WOA) 98 Sample software, which gives the area-weighted average of the 4 WOA temperature points surrounding the sample locations at 10-m water depth. The foraminiferal assemblages at Site U1305 were matched with the assemblages found in the modern core top database using the program Analog (31). Squared chord distance was used as the dissimilarity measure (29), while core tops with dissimilarity greater than 0.4 were not considered. The dissimilarity coefficient has a higher value when a similar analog in the core top database does not exist, suggesting a poor modern analog.

At Site U1305, the average dissimilarity coefficient through the 43.85- to 79.57-mcd interval (i.e., spanning MIS 7e through MIS 11c) is 0.048, with an SD of ~0.01. The averages of summer and winter SST SDs for MIS 7e are 0.98 and 1.7 °C, respectively; for MIS 9e, they are 0.91 and 1.38 °C, respectively, and for MIS 11c, they are 1.2 and 1.4 °C, respectively. Low dissimilarity coefficients (≤0.1) and low SD of the SST estimates derived from the top 5 best analogs suggest reliable SST estimates through most of MIS 9e and MIS 11c. High dissimilarity coefficients (≥0.2) for an interval during peak MIS 7e indicate poor modern analogs and lower confidence in the SST estimates for these samples (*SI Appendix*, Fig. S6). During cold intervals (e.g., Heinrich events), although the dissimilarity coefficients are low (≤0.1), the SDs of the SST estimates are high (~2 °C). This is most likely due to high abundance of *N. pachyderma* (s) (Figs. 1 and 3 and *SI Appendix*, Fig. S6), as ~100% *N. pachyderma* (s) abundance has a wider temperature range in the modern ocean (10, 11, 31–33).

**Mg/Ca.** Planktonic foraminifers *N. pachyderma* (s) and *N. incompta*, picked from the same samples used for foraminiferal assemblages and IRD counts, are used for Mg/Ca analysis. *N. pachyderma* (s) is a polar species, with calcification depths varying from the upper 50 m down to ~100 to 200 m (34–36). *N. pachyderma* (s) blooms during the spring and in late summer (35). However, as previously discussed in Irvalı et al. (10), at ~100 to 200 m, there is little change in seasonal temperatures, as these depths lie below the summer/seasonal thermocline; therefore, *N. pachyderma* (s)-based SST records (e.g., Mg/Ca) may also reflect annual or winter changes depending on depth habitat. This is consistent with our Mg/Ca-based SSTs following closely our MAT Winter SSTs (*SI Appendix*, Fig. S7*B*). Compared with *N. pachyderma* (s) (36), *N. incompta* calcifies at or above the pycnocline (above 150 m), preferring shallower and warmer surface waters (37, 38). Based on sediment trap studies, *N. incompta* blooms during late summer (July to September) at high latitudes (38) and follows closely our MAT summer SST estimates through the 4 previous interglacial plateaus (*SI Appendix*, Fig. S7*A*).

For Mg/Ca analysis, an average of ~75 to 90 individuals were picked from the 150- to 250-μm fraction. Using 2 clean glass slides, foraminiferal tests were gently crushed under a microscope to open the individual chambers and transferred into acid-leached vials. The crushed foraminiferal tests were cleaned using a cleaning protocol to remove clays, metal oxides, and organic matter followed by a weak acid leach and final dissolution in dilute $HNO_3$. Measurements were carried out following the method outlined by Rosenthal et al. (39) on a Finnigan MAT Element XR Sector Field Inductively Coupled Plasma Mass Spectrometer at the Department of Marine and Coastal Sciences, Rutgers, The State University of New Jersey.

Here, we applied the same approach following Irvalı et al. (10, 11) and converted our *N. pachyderma* (s)-derived Mg/Ca data to temperature estimates using the linear core top calibration equation developed by Kozdon et al. (40) (Fig. 1), which is based on the correlation with calcification temperatures inferred from Ca isotopes between 3 and 6 °C. To account for the difference in the cleaning protocol (reductive step), we corrected the intercept in the original calibration of Kozdon et al. (40) by −10% (41, 42) and used the following equation: $Mg/Ca = 0.13T + 0.32$. The choice of this equation and the limitation of the calibration are discussed in detail in Irvalı et al. (11). Considering all of the uncertainties in the calibration, the error on the combined calibration is about ±0.4 °C (1 standard error of the estimate, SEE) for temperatures >3 °C.

To convert our *N. incompta*-derived Mg/Ca data to temperature estimates, we further use the calibration developed by Morley et al. (37), and we used the equation $Mg/Ca = 0.40e^{(0.09T)}$ after correcting the Mg/Ca for the $[CO_3^{2-}]$ ion effect. The latter correction was done on B/Ca data obtained for these samples following the approach proposed by Morley et al. (37). Morley et al. (37) report a large calibration error on the order of ±2.78 °C, which they attribute to the limited data available to estimate the relationship between Mg/Ca and $CO_3$ ion concentration for values <200 μmol $kg^{-2}$. However, based on the comparison of downcore data between the 2 foraminifera species and the MAT results, we estimate our error in these records to be on the order of <±0.6 °C.

**Data Availability.** Proxy data are available in Dataset S1.

**ACKNOWLEDGMENTS.** We thank the scientific party and crew of R/V *JOIDES Resolution* IODP Expedition 303 and the curatorial staff at the IODP Bremen core repository for core sampling assistance. This study was funded through Research Council of Norway (RCN) THRESHOLDS Project Grant 254964. Stable isotope data were produced at the Facility for Advanced Isotopic Research and Monitoring of Weather, Climate and Biogeochemical Cycling (FARLAB; RCN Grant 245907).

1. P. Lemke *et al.*, "Observations: Changes in snow, ice and frozen ground" in *Climate Change 2007: The Physical Science Basis. Contribution of Working Group I to the Fourth Assessment Report of the Intergovernmental Panel on Climate Change*, S. Solomon *et al.*, Eds. (Cambridge University Press, Cambridge, UK, 2007), pp. 337–383.
2. A. Robinson, J. Alvarez-Solas, R. Calov, A. Ganopolski, M. Montoya, MIS-11 duration key to disappearance of the Greenland ice sheet. *Nat. Commun.* **8**, 16008 (2017).
3. A. Robinson, R. Calov, A. Ganopolski, Greenland ice sheet model parameters constrained using simulations of the Eemian Interglacial. *Clim. Past* **7**, 381–396 (2011).



Downloaded at UNIVERSITETSBIBL I BERGEN TIDSSKRIFT on January 14, 2020

4. E. J. Stone, D. J. Lunt, J. D. Annan, J. C. Hargreaves, Quantification of the Greenland ice sheet contribution to Last Interglacial sea level rise. *Clim. Past* **9**, 621–639 (2013).
5. A. de Vernal, C. Hillaire-Marcel, Natural variability of Greenland climate, vegetation, and ice volume during the past million years. *Science* **320**, 1622–1625 (2008).
6. A. V. Reyes *et al*., South Greenland ice-sheet collapse during Marine Isotope Stage 11. *Nature* **510**, 525–528 (2014).
7. J. M. Schaefer *et al*., Greenland was nearly ice-free for extended periods during the Pleistocene. *Nature* **540**, 252–255 (2016).
8. E. J. Colville *et al*., Sr-Nd-Pb isotope evidence for ice-sheet presence on southern Greenland during the Last Interglacial. *Science* **333**, 620–623 (2011).
9. R. G. Hatfield *et al*., Interglacial responses of the southern Greenland ice sheet over the last 430,000 years determined using particle-size specific magnetic and isotopic tracers. *Earth Planet. Sci. Lett.* **454**, 225–236 (2016).
10. N. Irvalı *et al*., Evidence for regional cooling, frontal advances, and East Greenland Ice Sheet changes during the demise of the last interglacial. *Quat. Sci. Rev.* **150**, 184–199 (2016).
11. N. Irvalı *et al*., Rapid switches in subpolar North Atlantic hydrography and climate during the Last Interglacial (MIS 5e). *Paleoceanography* **27**, PA2207 (2012).
12. J. M. Hall, L.-H. Chan, Ba/Ca in Neogloboquadrina pachyderma as an indicator of deglacial meltwater discharge into the western Arctic Ocean. *Paleoceanography* **19**, PA1017 (2004).
13. L. D. Trusel *et al*., Nonlinear rise in Greenland runoff in response to post-industrial Arctic warming. *Nature* **564**, 104–108 (2018).
14. M. Bevis *et al*., Accelerating changes in ice mass within Greenland, and the ice sheet's sensitivity to atmospheric forcing. *Proc. Natl. Acad. Sci. U.S.A.* **116**, 1934–1939 (2019).
15. J. Ridley, J. M. Gregory, P. Huybrechts, J. Lowe, Thresholds for irreversible decline of the Greenland ice sheet. *Clim. Dyn.* **35**, 1049–1057 (2010).
16. A. Robinson, R. Calov, A. Ganopolski, Multistability and critical thresholds of the Greenland ice sheet. *Nat. Clim. Chang.* **2**, 429–432 (2012).
17. A. Levermann, R. Winkelmann, A simple equation for the melt elevation feedback of ice sheets. *Cryosphere* **10**, 1799–1807 (2016).
18. H. F. Kleiven, U. S. Ninnemann, N. Irvalı, "Multi-proxy evidence for climate and North Atlantic Deep Water variability spanning the mid to late Holocene at the Erik sediment drift" in *Proceedings of the 2012 Fall Meeting AGU* (American Geophysical Union, 2012).
19. A. Landais *et al*., How warm was Greenland during the last interglacial period? *Clim. Past* **12**, 1933–1948 (2016).
20. A. Born, M. A. Imhof, T. F. Stocker, An efficient surface energy–mass balance model for snow and ice. *The Cryosphere* **13**, 1529–1546 (2019).
21. A. Plach *et al*., Eemian Greenland SMB strongly sensitive to model choice. *Clim. Past* **14**, 1463–1485 (2018).
22. A. Born, K. H. Nisancioglu, Melting of Northern Greenland during the last interglaciation. *Cryosphere* **6**, 1239–1250 (2012).
23. C. Contoux, C. Dumas, G. Ramstein, A. Jost, A. M. Dolan, Modelling Greenland ice sheet inception and sustainability during the Late Pliocene. *Earth Planet. Sci. Lett.* **424**, 295–305 (2015).
24. H. Fischer *et al*., Palaeoclimate constraints on the impact of 2 °C anthropogenic warming and beyond. *Nat. Geosci.* **11**, 474–485 (2018).
25. J. Hinkel *et al*., Coastal flood damage and adaptation costs under 21st century sea-level rise. *Proc. Natl. Acad. Sci. U.S.A.* **111**, 3292–3297 (2014).
26. J. Hansen *et al*., Young people's burden: Requirement of negative CO2 emissions. *Earth Syst. Dynam.* **8**, 577–616 (2017).
27. K. F. Darling, M. Kucera, D. Kroon, C. M. Wade, A resolution for the coiling direction paradox in *Neogloboquadrina pachyderma*. *Paleoceanography* **21**, PA2011 (2006).
28. W. H. Hutson, The agulhas current during the late pleistocene: Analysis of modern faunal analogs. *Science* **207**, 64–66 (1980).
29. W. L. Prell, *The Stability of Low-Latitude Sea Surface Temperatures: An Evaluation of the CLIMAP Reconstruction with Emphasis on the Positive SST Anomalies* (US Department of Energy, Washington, DC, 1985).
30. M. Kucera *et al*., Reconstruction of sea-surface temperatures from assemblages of planktonic foraminifera: Multi-technique approach based on geographically constrained calibration data sets and its application to glacial Atlantic and Pacific Oceans. *Quat. Sci. Rev.* **24**, 951–998 (2005).
31. W. L. Prell, A. Martin, J. Cullen, M. Trend, The Brown University Foraminiferal Data Base, IGBP PAGES/World Data Center-A for Paleoclimatology Data Contribution Series #1999-027 (NOAA/NGDC Paleoclimatology Program, Boulder CO, 1999). https://www.ncdc.noaa.gov/paleo-search/study/5908. Accessed 7 December 2010.
32. K. E. Kohfeld, R. G. Fairbanks, S. L. Smith, I. D. Walsh, *Neogloboquadrina pachyderma* (sinistral coiling) as paleoceanographic tracers in polar oceans: Evidence from Northeast Water Polynya plankton tows, sediment traps, and surface sediments. *Paleoceanography* **11**, 679–699 (1996).
33. D. W. Oppo, J. F. McManus, J. L. Cullen, Evolution and demise of the last interglacial warmth in the subpolar North Atlantic. *Quat. Sci. Rev.* **25**, 3268–3277 (2006).
34. D. Bauch, J. Carstens, G. Wefer, Oxygen isotope composition of living Neogloboquadrina pachyderma (sin.) in the Arctic Ocean. *Earth Planet. Sci. Lett.* **146**, 47–58 (1997).
35. L. Jonkers, G.-J. A. Brummer, F. J. C. Peeters, H. M. van Aken, M. F. De Jong, Seasonal stratification, shell flux, and oxygen isotope dynamics of left-coiling *N. pachyderma* and *T. quinqueloba* in the western subpolar North Atlantic. *Paleoceanography* **25**, PA2204 (2010).
36. J. Simstich, M. Sarnthein, H. Erlenkeuser, Paired δ18O signals of Neogloboquadrina pachyderma (s) and Turborotalita quinqueloba show thermal stratification structure in Nordic Seas. *Mar. Micropaleontol.* **48**, 107–125 (2003).
37. A. Morley *et al*., Environmental controls on Mg/Ca in Neogloboquadrina incompta: A core-top study from the subpolar North Atlantic. *Geochem. Geophys. Geosyst.* **18**, 4276–4298 (2017).
38. M. R. Chapman, Seasonal production patterns of planktonic foraminifera in the NE Atlantic Ocean: Implications for paleotemperature and hydrographic reconstructions. *Paleoceanography* **25**, PA1101 (2010).
39. Y. Rosenthal, M. P. Field, R. M. Sherrell, Precise determination of element/calcium ratios in calcareous samples using sector field inductively coupled plasma mass spectrometry. *Anal. Chem.* **71**, 3248–3253 (1999).
40. R. Kozdon, A. Eisenhauer, M. Weinelt, M. Y. Meland, D. Nürnberg, Reassessing Mg/Ca temperature calibrations of Neogloboquadrina pachyderma (sinistral) using paired delta(44/40)Ca and Mg/Ca measurements. *Geochem. Geophys. Geosyst.* **10**, 1–14 (2009).
41. M. Y. Meland *et al*., Mg/Ca ratios in the planktonic foraminifer *Neogloboquadrina pachyderma* (sinistral) in the northern North Atlantic/Nordic Seas. *Geochem. Geophys. Geosyst.* **7**, Q06P14 (2006).
42. Y. Rosenthal *et al*., Interlaboratory comparison study of Mg/Ca and Sr/Ca measurements in planktonic foraminifera for paleoceanographic research. *Geochem. Geophys. Geosyst.* **5**, Q04D09 (2004).
43. E. V. Galaasen *et al*., Rapid reductions in North Atlantic Deep Water during the peak of the last interglacial period. *Science* **343**, 1129–1132 (2014).



Downloaded at UNIVERSITETSBIBL I BERGEN TIDSSKRIFT on January 14, 2020